
On Accelerating Diffusion-Based Sampling Process via Improved Integration Approximation

Guoqiang Zhang

University of Technology Sydney
guoqiang.zhang@uts.edu.au

Kenta Niwa

NTT Communication Science Laboratories
kenta.niwa.bk@hco.ntt.co.jp

W. Bastiaan Kleijn

Victoria University of Wellington
bastiaan.kleijn@vuw.ac.nz

Abstract

One popular diffusion-based sampling strategy attempts to solve the reverse ordinary differential equations (ODEs) effectively. The coefficients of the obtained ODE solvers are pre-determined by the ODE formulation, the reverse discrete timesteps, and the employed ODE methods. In this paper, we consider accelerating several popular ODE-based sampling processes by optimizing certain coefficients via improved integration approximation (IIA). At each reverse timestep, we propose to minimize a mean squared error (MSE) function with respect to certain selected coefficients. The MSE is constructed by applying the original ODE solver for a set of fine-grained timesteps which in principle provides a more accurate integration approximation in predicting the next diffusion hidden state. Given a pre-trained diffusion model, the procedure for IIA for a particular number of neural functional evaluations (NFEs) only needs to be conducted once over a batch of samples. The obtained optimal solutions for those selected coefficients via minimum MSE (MMSE) can be restored and reused later on to accelerate the sampling process. Extensive experiments on EDM and DDIM show the IIA technique leads to significant performance gain when the numbers of NFEs are small.

1 Introduction

As one type of generative models, diffusion probabilistic models (DPMs) have made significant progress in recent years. The pioneering work [25] applied non-equilibrium statistical physics to estimating probabilistic data distributions. In doing so, a Markov forward diffusion process is constructed by systematically inserting additive noise into a data distribution until the data is almost destroyed. It is then gradually restored by a reverse diffusion process starting from a simple parametric distribution. The main advantage of DPMs over classic tractable models (e.g., HMMs, GMMs, see [5]) is that they can accurately model both the high and low likelihood regions of the data distribution via progressive estimation of noise-perturbed data distributions. In comparison to generative adversarial networks (GANs) [8; 1; 9; 24], DPMs exhibit more stable training dynamics by avoiding adversarial learning.

By following [25], different learning and/or sampling strategies have been proposed to improve the performance of DPMs, which include, for example, denoising diffusion probabilistic models (DDPMs) [10], denoising diffusion implicit models (DDIMs) [26], improved DDIMs [19; 7], latent diffusion models (LDMs)[22], score matching with Langevin dynamics (SMLD) [28; 27; 29], analytic-DPMs [4; 3], optimized denoising schedules [15; 6; 16], and guided diffusion strategies [20; 13]. It is worth noting that DDIM can be taken as the first-order ODE solver, where its coeffi-

clients are pre-determined by the ODE formulation and the discrete reverse timesteps. See also [31] for a detailed literature overview.

To further improve the sampling qualities in DPMs, one recent research trend is to exploit high-order methods for solving the ordinary differential equations (ODEs) in the sampling processes. The authors of [17] proposed pseudo numerical methods for diffusion models (PNDM), of which high-order polynomials of the estimated Gaussian noises from a score network are introduced per time-step to improve the sampling qualities. The work [34] further extends [17] by refining the coefficients of the high-order polynomials of the estimated Gaussian noises, and proposes diffusion exponential integrator sampler (DEIS). Recently, the authors of [18] considered solving the ODEs of a diffusion model differently from [34]. In particular, high-order Taylor expansion of the estimated Gaussian noises was employed to better approximate the continuous solutions of the ODEs, where the developed sampling method is referred to as DPM-Solver. The recent work [33] improves the sampling performance of DDPM, DDIM, 2nd order PNDM, DEIS, and DPM-Solver by performing additional extrapolation on the estimated clean data at each reverse timestep.

Surprisingly, the most recent work [12] achieves state-of-the-art (SOTA) sampling performance on CIFAR10 and ImageNet64 by utilizing only the improved Euler method (i.e., a classical 2nd order ODE solver [2]) to solve an ODE of a refined diffusion model, referred to as the EDM sampling procedure. The refined diffusion models are obtained in [12] via modifications of the neural architectures, novel ODE formulations, and proper parameter selections. Similarly to DDIM, the coefficients of EDM are pre-determined by the ODE formulation and the reverse timesteps.

In this paper, we consider accelerating several promising ODE-based sampling processes (including EDM and DDIM) for small numbers of neural function evaluations (NFEs), which is practically quite important for saving computational power. The basic idea of our approach is to improve the accuracy of the integration approximation when predicting the next diffusion hidden state by minimising a mean squared error (MSE) function, referred to as the *improved integration approximation* (IIA) technique. The MSE per reverse timestep is constructed by measuring the difference between the coarse and fine-grained approximations of an ODE integration, where the fine-grained approximation is obtained by applying the original ODE solver over a set of fine-grained timesteps. The MSE is then minimized with respect to certain selected coefficients embedded in the coarse integration approximation.

Given a pre-trained diffusion model, we emphasize that the optimal solutions of the MSEs only need to be computed once by using a batch of samples for a particular setup of reverse timesteps. As a result, the computational complexity of IIA can be ignored. After being obtained for the first time, they can be pre-stored together with the model and reused later for effective sampling later on. Extensive experiments over different pre-trained diffusion models demonstrate that IIA improves the sampling qualities of DDIM and EDM significantly when the numbers of NFEs are small.

2 Preliminary

Forward and reverse diffusion processes: Suppose the data sample \mathbf{x} follows a data distribution $p_{data}(\mathbf{x})$. A forward diffusion process adds Gaussian noises to the data samples \mathbf{x} progressively to obtain \mathbf{z}_t as t increases from 0 until T , of which the conditional distribution given \mathbf{x} can be represented as

$$q_{t|0}(\mathbf{z}_t|\mathbf{x}) = \mathcal{N}(\mathbf{z}_t|\alpha_t \mathbf{x}, \sigma_t^2 \mathbf{I}), \quad (1)$$

where α_t and σ_t are assumed to be differential functions of t with bounded derivatives. We use $q(\mathbf{z}_t; \alpha_t, \sigma_t)$ to denote the marginal distribution of \mathbf{z}_t . The samples of the distribution $q(\mathbf{z}_T; \alpha_T, \sigma_T)$ would be practically indistinguishable from pure Gaussian noises if $\sigma_T \gg \alpha_T$.

The reverse process of a diffusion model firstly draws a sample \mathbf{z}_T from $\mathcal{N}(\mathbf{0}, \sigma_T^2 \mathbf{I})$, and then progressively denoises it to obtain a sequence of denoised points $\{\mathbf{z}_{t_i} \sim p(\mathbf{z}; \alpha_{t_i}, \sigma_{t_i})\}_{i=0}^N$, where we use the notation $p(\cdot)$ to indicate that reverse sample distribution might not be identical to the forward distribution $q(\cdot)$ because of practical approximations. It is expected that the final sample \mathbf{z}_{t_N} is roughly distributed according to $p_{data}(\mathbf{x})$. Or equivalently, $p_{data}(\mathbf{x}) \approx p(\mathbf{z}_{t_N}; \alpha_{t_N}, \sigma_{t_N})$ where $t_N = 0$.

ODE formulation: To systematically characterize the forward and reverse diffusion processes, Song et al. [29] present a so-called *probability flow* ODE. With the formulation (1) for a forward

diffusion process, its reverse ODE form can be represented as

$$d\mathbf{z} = \left[f(t)\mathbf{z}_t - \frac{1}{2}g^2(t)\nabla_{\mathbf{z}} \log q(\mathbf{z}_t; \alpha_t, \sigma_t) \right] dt, \quad (2)$$

where the two functions $f(t)$ and $g(t)$ are represented in terms of (α_t, σ_t) as

$$f(t) = \frac{d \log \alpha_t}{dt}, \quad g^2(t) = \frac{d \sigma_t^2}{dt} - 2 \frac{d \log \alpha_t}{dt} \sigma_t^2. \quad (3)$$

$\nabla_{\mathbf{z}} \log q(\mathbf{z}; \alpha_t, \sigma_t)$ in (2) is the score function [11] pointing towards higher density of data samples at the given noise level (α_t, σ_t) . One nice property of the score function is that it does not depend on the generally intractable normalization constant of the underlying density function $q(\mathbf{z}; \alpha_t, \sigma_t)$, making it much easy for computation. The forward diffusion ODE can be simply obtained by putting a minus sign at the RHS of (2).

As t increases, the probability flow ODE (2) continuously reduces noise level of the data samples in the reverse process. In the ideal scenario where no approximations are introduced in (2), the sample distribution $p(\mathbf{z}; \alpha_t, \sigma_t)$ approaches to $p_{data}(\mathbf{x})$ as t goes from T to 0. As a result, the sampling process of a diffusion model boils down to solving the ODE form (2), where randomness is only introduced in the initial samples. This has opened up the research opportunity of exploiting different ODE solvers in diffusion-based sampling processes.

Denoising score matching: To be able to utilize (2) for sampling, one needs to specify a particular form of the score function $\nabla_{\mathbf{z}} \log q(\mathbf{z}; \alpha_t, \sigma_t)$. One common approach is to train a noise estimator $\hat{\epsilon}_{\theta}$ by minimizing the expected L_2 error for samples drawn from q_{data} (see [10; 29; 26]):

$$\mathbb{E}_{\mathbf{x} \sim p_{data}} \mathbb{E}_{\epsilon \sim \mathcal{N}(\mathbf{0}, \sigma_t^2 \mathbf{I})} \|\hat{\epsilon}_{\theta}(\alpha_t \mathbf{x} + \sigma_t \epsilon, t) - \epsilon\|_2^2, \quad (4)$$

where (α_t, σ_t) are from the forward process (1). The common practice in diffusion models is to utilize a neural network of U-Net architecture [23] to represent the noise estimator $\hat{\epsilon}_{\theta}$. With (4), the score function can then be represented in terms of $\hat{\epsilon}_{\theta}(\mathbf{z}_t; t)$ as

$$\nabla_{\mathbf{z}} \log q(\mathbf{z}_t; \alpha_t, \sigma_t) = -\hat{\epsilon}_{\theta}(\mathbf{z}_t; t) / \sigma_t. \quad (5)$$

Alternatively, the score function can be represented in terms of an estimator for \mathbf{x} (see [12]). The functional form for the noise level (α_t, σ_t) also plays an important role in the sampling qualities in practice. For example, the setup $(\alpha_t, \sigma_t) = (1, \sqrt{t})$ was studied in [29], which corresponds to constant-speed heat diffusion. The recent work [12] found that a simple form of $(\alpha_t, \sigma_t) = (1, t)$ works well in practice.

3 Improved Integration Approximation (IIA) for EDM

In this section, we first briefly review the EDM¹ sampling procedure for solving the ODE (2) in [12]. After that, we present the new technique of improved integration approximation (IIA) for solving the ODE in a more accurate manner when the numbers of NFEs are small.

3.1 Review of EDM sampling procedure in [12]

The recent work [12] reparameterizes the forward diffusion process (1) to be

$$q_{t|0}(\mathbf{z}_t | \mathbf{x}) = \mathcal{N}(\mathbf{z}_t | \alpha_t \mathbf{x}, \alpha_t^2 \tilde{\sigma}_t^2 \mathbf{I}), \quad (6)$$

where σ_t of (1) is represented as $\sigma_t = \alpha_t \tilde{\sigma}_t$. Let $\mathbf{D}_{\theta}(\mathbf{z}_t, t)$ denote an estimator for the data sample \mathbf{x} at timestep t . It can be computed in terms of the noise estimator $\hat{\epsilon}_{\theta}$ as $\mathbf{D}_{\theta}(\mathbf{z}_t, t) = \mathbf{z}_t / \alpha_t - \tilde{\sigma}_t \hat{\epsilon}_{\theta}(\mathbf{z}_t, t)$. The resulting probability flow ODE takes the form of

$$d\mathbf{z} = \left[\frac{\dot{\alpha}_t}{\alpha_t} \mathbf{z}_t - \alpha_t^2 \dot{\tilde{\sigma}}_t \tilde{\sigma}_t \nabla_{\mathbf{z}} \log q(\mathbf{z}_t; \alpha_t, \alpha_t \tilde{\sigma}_t) \right] dt = \underbrace{\left[\left(\frac{\dot{\alpha}_t}{\alpha_t} + \frac{\dot{\tilde{\sigma}}_t}{\tilde{\sigma}_t} \right) \mathbf{z} - \frac{\dot{\tilde{\sigma}}_t \alpha_t}{\tilde{\sigma}_t} \mathbf{D}_{\theta}(\mathbf{z}_t, t) \right]}_{\mathbf{d}(\mathbf{z}, t)} dt, \quad (7)$$

¹It is not explicitly explained in [12] what does the notation EDM refer to, or at least we did not find its physical meaning.

Algorithm 1 Basic IIA-EDM as an extension of EDM in [12]

```

1: Input:
2: number of time steps  $N$ ,  $\{\gamma_{ik}^*|k=0,1,\dots,r\}_{i=0}^{N-2}$  [pre-computed values obtained via MMSE]
3: Sample  $\mathbf{z}_0 \sim \mathcal{N}(\mathbf{0}, \alpha_{t_0}^2 \tilde{\sigma}_{t_0}^2 \mathbf{I})$ 
4: for  $i \in \{0, 1, \dots, N-1\}$  do
5:    $\mathbf{d}_i \leftarrow \left( \frac{\dot{\sigma}_{t_i}}{\tilde{\sigma}_{t_i}} + \frac{\dot{\alpha}_{t_i}}{\alpha_{t_i}} \right) \mathbf{z}_i - \frac{\dot{\sigma}_{t_i} \alpha_{t_i}}{\tilde{\sigma}_{t_i}} D_{\theta}(\mathbf{z}_i; t_i)$ 
6:    $\tilde{\mathbf{z}}_{i+1} \leftarrow \mathbf{z}_i + (t_{i+1} - t_i) \mathbf{d}_i$ 
7:   if  $\sigma_{t_{i+1}} \neq 0$  then
8:      $\mathbf{d}'_{i+1|i} \leftarrow \left( \frac{\dot{\sigma}_{t_{i+1}}}{\tilde{\sigma}_{t_{i+1}}} + \frac{\dot{\alpha}_{t_{i+1}}}{\alpha_{t_{i+1}}} \right) \tilde{\mathbf{z}}_{i+1} - \frac{\dot{\sigma}_{t_{i+1}} \alpha_{t_{i+1}}}{\tilde{\sigma}_{t_{i+1}}} D_{\theta}(\tilde{\mathbf{z}}_{i+1}; t_{i+1})$ 
9:      $\mathbf{z}_{i+1} \leftarrow \mathbf{z}_i + (t_{i+1} - t_i) \sum_{k=0}^r \gamma_{ik}^* \left( \frac{1}{2} \mathbf{d}_{i-k} + \frac{1}{2} \mathbf{d}'_{i-k+1|i-k} \right)$  [historical gradients are used]
10:  end if
11: end for
12: Output:  $\mathbf{z}_N$ 

```

Remark: Sampling of [12] is recovered when $\{\gamma_{i0}^* = 1\}_{i=0}^{N-2}$ and $\{\gamma_{ik}^* = 0|k \neq 0\}_{i=0}^{N-2}$.

where the dot operation denotes a time derivative, and the gradient $\frac{d\mathbf{z}}{dt}$ is represented by $\mathbf{d}(\mathbf{z}, t)$.

The work [12] proposed a deterministic sampling procedure for solving (7) with arbitrary $\tilde{\sigma}_t$ and α_t . Basically, the improved Euler (a.k.a. Heun's 2nd order method [2]) was utilized for solving the ODE form, of which the update expressions from time t_i to t_{i+1} are given by

$$\tilde{\mathbf{z}}_{i+1} = \mathbf{z}_i + (t_{i+1} - t_i) \mathbf{d}_i \quad (8)$$

$$\mathbf{z}_{i+1} = \mathbf{z}_i + (t_{i+1} - t_i) \left(\frac{1}{2} \mathbf{d}_i + \frac{1}{2} \mathbf{d}'_{i+1|i} \right), \quad (9)$$

where $(t_{i+1} - t_i)$ is the stepsize, $\mathbf{d}_i = \mathbf{d}(\mathbf{z}_i, t_i)$, and $\mathbf{d}'_{i+1|i} = \mathbf{d}(\tilde{\mathbf{z}}_{i+1}, t_{i+1})$. $\tilde{\mathbf{z}}_{i+1}$ is the intermediate estimate of the hidden state \mathbf{z} at time t_{i+1} . The final estimate \mathbf{z}_{i+1} is computed by utilizing the average of the gradients \mathbf{d}_i and $\mathbf{d}'_{i+1|i}$. Or equivalently, the associated integration $\int_{t_i}^{t_{i+1}} \mathbf{d}(\mathbf{z}, t) dt$ of (7) is approximated as

$$\int_{t_i}^{t_{i+1}} \mathbf{d}(\mathbf{z}, t) dt \approx (t_{i+1} - t_i) \left(\frac{1}{2} \mathbf{d}_i + \frac{1}{2} \mathbf{d}'_{i+1|i} \right). \quad (10)$$

Its sampling procedure is a special case of Alg. 1 by manually setting $\{\gamma_{i0}^* = 1\}_{i=0}^{N-2}$ and $\{\gamma_{ik}^* = 0|k \neq 0\}_{i=0}^{N-2}$. We will explain in the next subsection how the set of parameters $\{\gamma_{ik}^*|k=0,\dots,r\}_{i=0}^{N-2}$ are computed by utilizing the IIA technique.

It is found in [12] that with the simple setup of $\sigma_t = t$ and $\alpha_t = 1$, the SOTA sampling performance is achieved by the EDM sampling procedure over CIFAR10 and ImageNet64. The authors of [12] carefully selected the discrete time steps (i.e., $t_{i < N}$ in Alg. 1) and a set of hyper-parameters, which is crucial for improving the sampling qualities.

3.2 Basic IIA for EDM via MMSE

In this subsection, we consider improving the accuracy of the integration approximation in (10) at timestep t_i . To do so, we propose to approximate the integration $\int_{t_i}^{t_{i+1}} \mathbf{d}(\mathbf{z}, t) dt$ by utilizing the most recent set of gradients $\{0.5 \mathbf{d}_{i-k} + 0.5 \mathbf{d}'_{i-k+1|i-k}\}_{k=0}^r$, given by

$$\int_{t_i}^{t_{i+1}} \mathbf{d}(\mathbf{z}, t) dt \approx \sum_{k=0}^r \gamma_{ik} \underbrace{(t_{i+1} - t_i)(0.5 \mathbf{d}_{i-k} + 0.5 \mathbf{d}'_{i-k+1|i-k})}_{\Delta_i(\mathbf{z}_{i-k})}, \quad (11)$$

where the set of scalars $\{\gamma_{ik}\}_{k=0}^r$ can be interpreted as the adaptive stepsizes being multiplied by those gradients. We attempt to find a proper setup for $\{\gamma_{ik}\}_{k=0}^r$ so that the integration approximation (11) will become more accurate than (10).

Our motivation for utilizing the most recent $r+1$ gradients in (11) is inspired by SGD with momentum [30; 21] and its variants [14; 32] which computes and makes use of the exponential moving

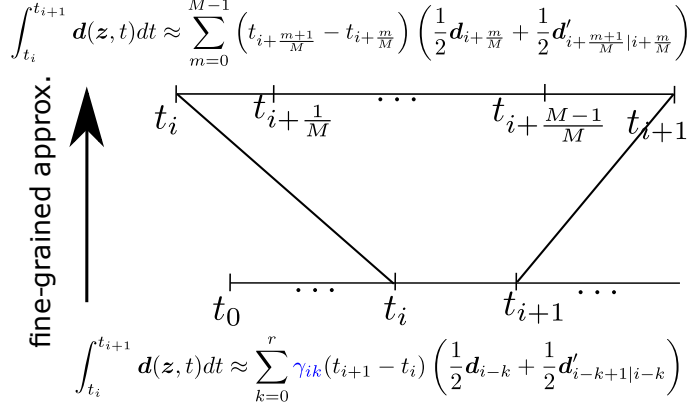


Figure 1: Coarse and fine-grained approximations of the integration $\int_{t_i}^{t_{i+1}} d(\mathbf{z}, t) dt$. $\{\gamma_{ik}\}_{k=0}^r$ are the introduced adaptive stepsizes, which remain to be determined.

average of historical gradients in updating machine learning models. In general, the recent gradients provide additional directions pointing towards lower functional values. Proper exploration of those gradients would help to accelerate the convergence speed.

We are now in a position to compute $\{\gamma_{ik}\}_{k=0}^r$ in (11) at timestep t_i . We note that the integration $\int_{t_i}^{t_{i+1}} d(\mathbf{z}, t) dt$ can be better approximated by applying the improved Euler method over a set of fine-grained timesteps $\{t_{i+\frac{m}{M}}\}_{m=0}^M$, where $m = 0$ and $m = M$ correspond to the starting time t_i and ending time t_{i+1} , respectively. Mathematically, the integration $\int_{t_i}^{t_{i+1}} d(\mathbf{z}, t) dt$ can be estimated more accurately over $\{t_{i+\frac{m}{M}}\}_{m=0}^M$ as

$$\begin{aligned} \int_{t_i}^{t_{i+1}} d(\mathbf{z}, t) dt &= \sum_{m=0}^{M-1} \int_{t_{i+\frac{m}{M}}}^{t_{i+\frac{m+1}{M}}} d(\mathbf{z}, t) dt \\ &\approx \sum_{m=0}^{M-1} \left(t_{i+\frac{m+1}{M}} - t_{i+\frac{m}{M}} \right) \left(0.5 \mathbf{d}_{i+\frac{m}{M}} + 0.5 \mathbf{d}'_{i+\frac{m+1}{M}|i+\frac{m}{M}} \right) \\ &= \Delta_{fg}(\mathbf{z}_i), \end{aligned} \quad (12)$$

where we use $\Delta_{fg}(\mathbf{z}_i)$ to denote the summation of the fine-grained integration approximations.

We compute the optimal solution of $\{\gamma_{ik}\}_{k=0}^r$ in (11) by minimizing the MSE with regard to the difference of the two approximations $\sum_{k=0}^r \gamma_{ik} \Delta_i(\mathbf{z}_{i-k})$ and $\Delta_{fg}(\mathbf{z}_i)$:

$$\{\gamma_{ik}^*\}_{k=0}^r = \arg \min \mathbb{E}_{\mathbf{z}_{t_0} \sim \mathcal{N}(0, \sigma_T^2 \mathbf{I})} \left\| \sum_{k=0}^r \gamma_{ik} \Delta_i(\mathbf{z}_{i-k}) - \Delta_{fg}(\mathbf{z}_i) \right\|^2, \quad (13)$$

where $\{\mathbf{z}_{i-k}\}_{k=0}^r$ are implicitly determined by the initial state \mathbf{z}_{t_0} in the deterministic sampling procedure. That is, the optimal adaptive stepsizes $\{\gamma_{ik}^*\}_{k=0}^r$ in (13) are computed by taking into account the probability distribution of the initial state \mathbf{z}_{t_0} . We note that the FID score for measuring image qualities is in fact also performed over the probability distribution of the initial state. In principle, if the MSE on the RHS of (13) is indeed reduced due to the solution $\{\gamma_{ik}^*\}_{k=0}^r$, the resulting FID should be improved.

In practice, one can solve the optimization problem (13) by utilizing a batch \mathcal{B} of initial samples at timestep t_0 to approximate the expectation operation. The solution $\{\gamma_{ik}^*\}_{k=0}^r$ can then be easily computed by minimizing a quadratic function. Consider the simple case of $r = 0$ as an example, where only the quantity $\Delta_i(\mathbf{z}_i)$ is employed in (13). The optimal solution γ_{i0}^* can be easily computed to be

$$\gamma_{i0}^* \approx \frac{\sum_{\mathbf{z}_{t_0} \in \mathcal{B}} \langle \Delta_i(\mathbf{z}_i), \Delta_{fg}(\mathbf{z}_i) \rangle}{\sum_{\mathbf{z}_{t_0} \in \mathcal{B}} \|\Delta_i(\mathbf{z}_i)\|^2}, \quad (14)$$

where $\langle \cdot \rangle$ denotes inner product.

3.3 Advanced IIA for EDM via MMSE

In this subsection, we present an advanced IIA technique for EDM. To do so, we reformulate the update expression for \mathbf{z}_{i+1} in (9) under the configuration of $\alpha_t = 1$. The resulting update expression is summarized in a lemma below:

Lemma 1. *The update expression for \mathbf{z}_{i+1} at timestep t_i in EDM under the configuration of $\alpha_t = 1$ can be reformulated to be*

$$\mathbf{z}_{i+1} = \mathbf{z}_i + (t_{i+1} - t_i) \bar{\mathbf{d}}_i \quad (15)$$

$$\bar{\mathbf{d}}_i = (\mathbf{z}_i - \bar{\mathbf{D}}_{\theta}(\mathbf{z}_i, \tilde{\mathbf{z}}_{i+1}))/t_i \quad (16)$$

$$\bar{\mathbf{D}}_{\theta}(\mathbf{z}_i, \tilde{\mathbf{z}}_{i+1}) = \mathbf{D}_{\theta}(\mathbf{z}_i; t_i) + \frac{t_i}{2t_{i+1}} [\mathbf{D}_{\theta}(\tilde{\mathbf{z}}_{i+1}; t_{i+1}) - \mathbf{D}_{\theta}(\mathbf{z}_i; t_i)], \quad (17)$$

where the detailed derivation is provided in Appendix A.

Lemma 1 indicates that the computation for \mathbf{z}_{i+1} can be decomposed into two steps. Firstly, a new estimator $\bar{\mathbf{D}}_{\theta}(\mathbf{z}_i, \tilde{\mathbf{z}}_{i+1})$ is computed via a gradient descent with stepsize $t_i/(2t_{i+1})$ in (17), where the quantity $[\mathbf{D}_{\theta}(\tilde{\mathbf{z}}_{i+1}; t_{i+1}) - \mathbf{D}_{\theta}(\mathbf{z}_i; t_i)]$ can be interpreted as a gradient vector pointing towards some data sample \mathbf{x} (see [33] for a detailed discussion). After that, \mathbf{z}_{i+1} is updated via another gradient descent operation in (15) with the stepsize $(t_{i+1} - t_i)$, where the gradient $\bar{\mathbf{d}}_i$ is computed by utilizing the new estimator $\bar{\mathbf{D}}_{\theta}(\mathbf{z}_i, \tilde{\mathbf{z}}_{i+1})$.

We propose to introduce additional adaptive stepsizes in front of the two quantities: $(\mathbf{z}_i - \mathbf{D}_{\theta}(\mathbf{z}_i; t_i))$ and $(\mathbf{D}_{\theta}(\tilde{\mathbf{z}}_{i+1}; t_{i+1}) - \mathbf{D}_{\theta}(\mathbf{z}_i; t_i))$. As will be explained below, the adaptive stepsizes will be determined by the improved integration approximation (IIA) technique. Specifically, we approximate the integration $\int_{t_i}^{t_{i+1}} \mathbf{d}(\mathbf{z}, t) dt$ at timestep t_i to be

$$\begin{aligned} \int_{t_i}^{t_{i+1}} \mathbf{d}(\mathbf{z}, t) dt &\approx (t_{i+1} - t_i) \left[\beta_{i0} (\mathbf{z}_i - \mathbf{D}_{\theta}(\mathbf{z}_i; t_i)) - \frac{\beta_{i1}}{2t_{i+1}} [\mathbf{D}_{\theta}(\tilde{\mathbf{z}}_{i+1}; t_{i+1}) - \mathbf{D}_{\theta}(\mathbf{z}_i; t_i)] + \sum_{k=1}^r \gamma_{ik} \tilde{\Delta}_{i-k} \right] \\ &= S_i(\beta_{i0}, \beta_{i1}, \{\gamma_{ik}\}_{k=1}^r | \mathbf{z}_i, \tilde{\mathbf{z}}_{i+1}), \end{aligned} \quad (18)$$

where $\tilde{\Delta}_{i-k} = \beta_{(i-k)0}^* (\mathbf{z}_{i-k} - \mathbf{D}_{\theta}(\mathbf{z}_{i-k}; t_{i-k})) - \frac{\beta_{(i-k)1}^*}{2t_{i-k+1}} [\mathbf{D}_{\theta}(\tilde{\mathbf{z}}_{i-k+1}; t_{i-k+1}) - \mathbf{D}_{\theta}(\mathbf{z}_{i-k}; t_{i-k})]$ denotes the gradient obtained previously at timestep t_{i-k} , of which $\beta_{(i-k)0}^*$ and $\beta_{(i-k)1}^*$ are the pre-determined adaptive stepsizes by minimizing an MSE at time-step t_{i-k} . It is noted that a number of most recent gradients $\{\tilde{\Delta}_{i-k}\}_{k=1}^r$ are also included in (18) for the purpose of providing additional gradient directions in the MSE minimisation below.

Next we compute the optimal stepsizes in the above function $S_i(\cdot)$ by minimizing an MSE :

$$(\beta_{i0}^*, \beta_{i1}^*, \{\gamma_{ik}^*\}_{i=1}^r) = \arg \min \mathbb{E}_{\mathbf{z}_{t_0} \sim \mathcal{N}(0, \sigma_T^2 \mathbf{I})} \|S_i(\beta_{i0}, \beta_{i1}, \{\gamma_{ik}\}_{k=1}^r | \mathbf{z}_i, \tilde{\mathbf{z}}_{i+1}) - \Delta_{fg}(\mathbf{z}_i)\|^2, \quad (19)$$

where $\Delta_{fg}(\mathbf{z}_i)$ is from (12). Since $S_i(\cdot)$ is a linear function of its variables, the optimal solution in (19) can be easily computed by minimizing a quadratic function. Similarly to the earlier subsection, the expectation operation in (19) can be approximated by utilizing a batch \mathcal{B} of initial samples at timestep t_0 . Again the optimisation (19) only needs to be performed once. Then the obtained optimal stepsizes can be prestored and reused later on in the sampling procedure.

By inspection (13) and (19), we can conclude that the optimisation (19) exploits the internal structure of the update for \mathbf{z}_{i+1} in EDM. For the special case of $r = 0$, (19) involves two variables (β_{i0}, β_{i1}) while (13) only consists of one variable γ_{i0} . Intuitively speaking, the residual error of (19) after minimisation should be smaller than that of (13), which would lead to improved sampling qualities.

4 Improved Integration Approximation (IIA) for DDIM

In this section, we consider applying the IIA technique for DDIM. We are aware that different high-order ODE solvers have already been proposed to improve the sampling performance of DDIM. Our objective is to find out if the IIA technique can also serve the same purpose.

The DDIM sampling procedure is in fact the first-order solver for the ODE formulation (2)-(3) (see [18; 34]). Its update expression is given by

$$z_{i+1} = \alpha_{t_{i+1}} \overbrace{\left(\frac{z_i - \sigma_{t_i} \hat{\epsilon}_{\theta}(z_i, t_i)}{\alpha_{t_i}} \right)}^{\hat{x}(z_i, t_i)} + \sigma_{t_{i+1}} \hat{\epsilon}_{\theta}(z_i, t_i) \quad (20)$$

$$\approx e^{\int_{t_i}^{t_{i+1}} f(\tau) d\tau} z_i + \int_{t_i}^{t_{i+1}} \left(e^{\int_{t_i}^{t_{i+1}} f(r) dr} \frac{g^2(\tau)}{2\sigma_{\tau}} \hat{\epsilon}_{\theta}(z_{\tau}, \tau) \right) d\tau, \quad (21)$$

where the estimator $\hat{x}(z_i, t_i)$ plays a similar role as $D_{\theta}(z_i, t_i)$ in EDM.

We now introduce two additional terms in computing z_{i+1} , which is given by

$$z_{i+1} = \underbrace{\alpha_{t_{i+1}} \hat{x}(z_i, t_i) + \sigma_{t_{i+1}} \hat{\epsilon}_{\theta}(z_i, t_i)}_{\text{1st term}} + \underbrace{\phi_{i0}^* (\hat{x}(z_i, t_i) - \hat{x}(z_{i-1}, t_{i-1}))}_{\text{2nd term}} + \underbrace{\phi_{i1}^* (\hat{\epsilon}_{\theta}(z_i, t_i) - \hat{\epsilon}_{\theta}(z_{i-1}, t_{i-1}))}_{\text{2nd term}}. \quad (22)$$

The first term in (22) can be interpreted as a gradient vector pointing towards the data sample x (see [33] and also (18) for advanced IIA-EDM). The second term in (22) is a vector measuring the difference of the noise estimators at timesteps t_i and t_{i-1} , which is inspired by those high-order ODE solvers [34; 17]. The two adaptive stepsizes $(\phi_{i0}^*, \phi_{i1}^*)$ in front of the two additional terms in (22) are computed by solving the following MSE problem:

$$(\phi_{i0}^*, \phi_{i1}^*) = \arg \min \mathbb{E}_{z_{t_0} \sim \mathcal{N}(0, \sigma_T^2 I)} \left\| \Phi_{t_i \rightarrow t_{i+1}}(z_i, t_i) + \phi_{i0} (\hat{x}(z_i, t_i) - \hat{x}(z_{i-1}, t_{i-1})) \right. \\ \left. + \phi_{i1} (\hat{\epsilon}_{\theta}(z_i, t_i) - \hat{\epsilon}_{\theta}(z_{i-1}, t_{i-1})) - \sum_{m=0}^{M-1} \Phi_{t_{i+\frac{m}{M}} \rightarrow t_{i+\frac{m+1}{M}}} (z_{i+\frac{m}{M}}, t_{i+\frac{m}{M}}) \right\|^2, \quad (23)$$

where the summation in the RHS of (23) from $m = 0$ until $m = M - 1$ corresponds to applying DDIM over a fine-grained set of timesteps $\{t_{i+\frac{m}{M}}\}_{m=0}^M$ within the time-interval of $[t_i, t_{i+1}]$. In principle, when M goes to infinity, the summation would provide a very accurate approximation of the integration in (21). The solution $(\phi_{i0}^*, \phi_{i1}^*)$ makes the update z_{i+1} in (22) optimal with respect to the MMSE criterion of (23). Again, the expectation in (23) can be realized by utilizing a batch \mathcal{B} of initial samples at t_0 .

Remark 1. We have also considered applying IIA for the high-order methods SPNDM and IPNDM. See the performance results in Appendix C. In brief, the IIA technique improves the sampling performance of SPNDM and IPNDM for certain pre-trained models. While for some pre-trained models, the FID scores of SPNDM and IPNDM first decreases then increases as the number of timesteps increases, which might be due to the improper selection of reverse timesteps. In these scenarios, the IIA technique does not help with the sampling qualities.

5 Experiments

We investigated the performance gain of the IIA technique when being implemented in both the EDM and DDIM sampling procedures. For the EDM sampling procedure, two IIA techniques are proposed. The associated sampling procedures are referred to as BIIA-EDM and IIA-EDM, where the notation 'BIIA' stands for the basic IIA. As we mentioned earlier, the optimal stepsizes for each pre-trained model over a particular set of reverse timesteps was only computed once, and were then stored and used for generating 50K images in computation of the FID score. It is found that the IIA technique significantly improves the sampling qualities for small numbers of NFEs (e.g., less than 30).

5.1 Performance of IIA based EDM

In this experiment, we tested four pre-trained models for four datasets: CIFAR10, FFHQ, AFHQV2, and ImageNet64. The batchsize $|\mathcal{B}|$ for computing the optimal adaptive stepsizes when employing both the basic and advanced IIA techniques was set to $|\mathcal{B}| = 200$, which is also the default minibatch

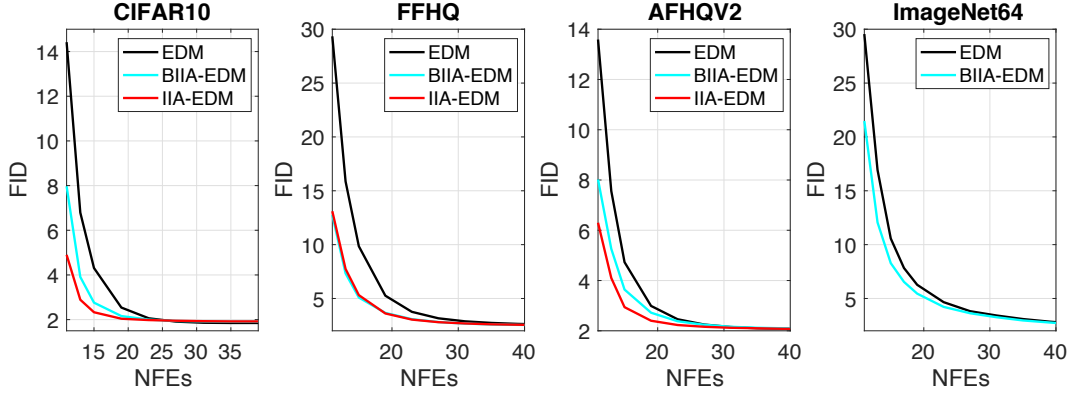


Figure 2: Performance of EDM, BIIA-EDM, and IIA-EDM.

size in the EDM official open-source repository. The other hyperparameters when minimizing the MSEs can be found in Table 1 of Appendix B.

Fig. 2 visualizes the FID scores for the four pre-trained models. It is clear that BIIA-EDM and IIA-EDM consistently outperform the EDM sampling procedure when the number of NFEs are smaller than 25. This can be easily explained by the fact that for a small number of NFEs, the integration approximation in EDM is not accurate. Both BIIA-EDM and IIA-EDM improve the accuracy of the integration approximation by introducing adaptive stepsizes. Furthermore, for the datasets of CIFAR10 and AFHQV2, IIA-EDM outperforms BIIA-EDM remarkably.

5.2 Performance of IIA based DDIM

In the second experiment, we study the performance gain of IIA-DDIM in comparison to DDIM. We tested three pre-trained models, one for a particular dataset: CIFAR10, LSUN bedroom, and LSUN church. The batchsize $|\mathcal{B}|$ for approximating the expectation operation in (23) was set 16, which is also the mini-batch size for sampling in computation of the FID scores. The hyper-parameter M in (23) was set to $M = 3$.

The performance results of DDIM and IIA-DDIM are visualized in Fig. 3. It is seen that IIA-DDIM outperforms DDIM consistently for different number of NFEs and across different pre-trained models. See also Fig. 4 in the appendix for the performance of IIA-SPNDM and IIA-IPNDM.

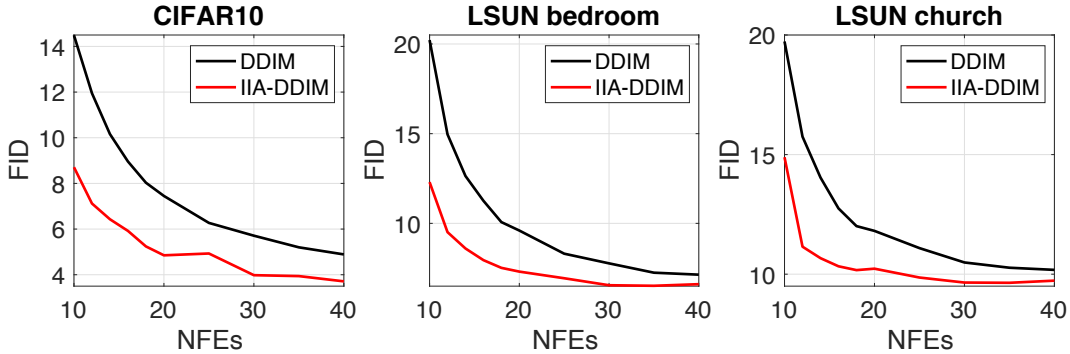


Figure 3: Performance of DDIM and IIA-DDIM.

6 Conclusions

In this paper, we have proposed a new technique of improved integration approximation (IIA) to accelerate the diffusion-based sampling processes. In particular, we have proposed to introduce additional adaptive stepsizes in existing popular ODE solvers in order to improve the accuracy of

integration approximation. The adaptive stepsizes at timestep t_i are determined by pushing a coarse integration approximation over $[t_i, t_{i+1}]$ to get closer to a highly accurate integration approximation over the same time slot. The adaptive stepsizes only need to be computed once and can then be stored and reused later on for extensive sampling.

Extensive experiments confirm that the IIA technique is able to significantly improve the sampling qualities of EDM and DDIM when the number of the NFEs are small (e.g., less than 30). This can be explained by the fact that the integration approximation in the original method for small numbers of NFEs is a rough estimate. Employment of IIA has significantly improves the accuracy of the integration approximation.

Additional experiments on applying IIA to the high-order methods SPNDM and IPNDM were also conducted. It is the found that IIA improves the performance only when the FID scores keep decreasing as the timesteps increases in the original sampling method.

References

- [1] M. Arjovsky, S. Chintala, and L. Bottou. Wasserstein GAN. arXiv:1701.07875 [stat.ML], 2017.
- [2] U. M. Ascher and L. R. Petzold. *Computer Methods for Ordinary Differential Equations and Differential-Algebraic Equations*. Soceity for Industrial and Applied Mathematics, 1998.
- [3] F. Bao, C. Li, J. Sun, J. Zhu, and B. Zhang. Estimating the Optimal Covariance with Imperfect Mean in Diffusion Probabilistic Models. In *ICML*, 2022.
- [4] F. Bao, C. Li, J. Zhu, and B. Zhang. Analytic-DPM: an Analytic Estimate of the Optimal Reverse Variance in Diffusion Probabilistic Models. In *ICLR*, 2022.
- [5] C. M. Bishop. *Pattern Recognition and Machine Learning*. Springer, 2006.
- [6] N. Chen, Y. Zhang, H. Zen, R. J. Weiss, M. Norouzi, and W. Chan. WaveGrad: Estimating Gradients for Waveform Generation. arXiv:2009.00713, September 2020.
- [7] P. Dhariwal and A. Nichol. Diffusion models beat gans on image synthesis. arXiv:2105.05233 [cs.LG], 2021.
- [8] I. Goodfellow, J. Pouget-Abadie, M. Mirza, B. Xu, D. Warde-Farley, S. Ozair, A. Courville, and Y. Bengio. Generative Adversarial Nets. In *Proceedings of the International Conference on Neural Information Processing Systems*, pages 2672–2680, 2014.
- [9] I. Gulrajani, F. Ahmed, M. Arjovsky, V. Dumoulin, and A. C. Courville. Improved training of wasserstein gans. In *Advances in neural information processing systems*, pages 5767–5777, 2017.
- [10] J. Ho, A. Jain, and P. Abbeel. Denoising diffusion probabilistic models. In *NeurIPS*, 2020.
- [11] A. Hyvarinen. Estimation of non-normalized statistical models by score matching. *Journal of Machine Learning Research*, 24:695–709, 2005.
- [12] T. Karras, M. Aittala, T. Alia, and S. Laine. Elucidating the Design Space of Diffusion-Based Generative Models. In *36th Conference on Nueral Information Processing Systems (NeurIPS)*, 2022.
- [13] D. Kim, Y. Kim, S. J. Kwon, W. Kang, and I.-C. Moon. Refining Generative Process with Discriminator Guidance in Score-based Diffusion Models. arXiv preprint arXiv:2211.17091 [cs.CV], 2022.
- [14] D. P. Kingma and J. L. Ba. Adam: A Method for Stochastic Optimization. arXiv preprint arXiv:1412.6980v9, 2017.
- [15] D. P. Kingma, T. Salimans, B. Poole, and J. Ho. Variational diffusion models. arXiv: preprint arXiv:2107.00630, 2021.

- [16] M. W. Y. Lam, J. Wang, D. Su, and D. Yu. BDDM: Bilateral Denoising Diffusion Models for Fast and High-Quality Speech Synthesis. In *ICLR*, 2022.
- [17] L. Liu, Y. Ren, Z. Lin, and Z. Zhao. Pseudo Numerical Methods for Diffusion Models on Manifolds. In *ICLR*, 2022.
- [18] C. Lu, Y. Zhou, F. Bao, J. Chen, C. Li, and J. Zhu. DPM-Solver: A Fast ODE Solver for Diffusion Probabilistic Sampling in Around 10 Steps. In *NeurIPS*, 2022.
- [19] A. Nichol and P. Dhariwal. Improved denoising diffusion probabilistic models. arXiv preprint arXiv:2102.09672, 2021.
- [20] A. Nichol, P. Dhariwal, A. Ramesh, P. Shyam, P. Mishkin, B. McGrew, I. Sutskever, and M. Chen. GLIDE: Towards Photorealistic image generation and editing with text-guided diffusion models. In *ICML*, 2022.
- [21] B. T. Polyak. Some methods of speeding up the convergence of iteration methods. *USSR Computational Mathematics and Mathematical Physics*, 4:1–17, 1964.
- [22] R. Rombach, A. Blattmann, D. Lorenz, P. Esser, and B. Ommer. High-resolution image synthesis with latent diffusion models. In *CVPR*, 2022.
- [23] O. Ronneberger, P. Fischer, and T. Brox. U-Net: Convolutional Networks for Biomedical Image Segmentation. arXiv:1505.04597 [cs.CV], 2015.
- [24] A. Sauer, K. Schwarz, and A. Geiger. StyleGAN-XL: Scaling StyleGAN to large diverse datasets. In *SIGGRAPH*, 2022.
- [25] J. Sohl-Dickstein, E. Weiss, N. Maheswaranathan, and S. Ganguli. Deep unsupervised learning using nonequilibrium thermodynamics. *ICML*, 2015.
- [26] J. Song, C. Meng, and S. Ermon. Denoising Diffusion Implicit Models. In *ICLR*, 2021.
- [27] Y. Song, C. Durkan, I. Murray, and S. Ermon. Maximum likelihood training of score-based diffusion models. In *Advances in neural information processing systems (NeurIPS)*, 2021.
- [28] Y. Song and S. Ermon. Generative modeling by estimating gradients of the data distribution. In *Advances in neural information processing systems (NeurIPS)*, page 11895–11907, 2019.
- [29] Y. Song, J. S.-Dickstein, D. P. Kingma, A. Kumar, S. Ermon, and B. Poole. Score-Based Generative Modeling Through Stochastic Differential Equations. In *ICLR*, 2021.
- [30] H. Sutskever, J. Martens, G. Dahl, and G. Hinton. On the importance of initialization and momentum in deep learning. In *International conference on Machine Learning (ICML)*, 2013.
- [31] L. Yang, Z. Zhang, S. Hong, R. Xu, Y., Y. Shao, W. Zhang, M.-H. Yang, and B. Cui. Diffusion models: A comprehensive survey of methods and applications. arXiv preprint arXiv:2102.09672, 2021.
- [32] G. Zhang. On Suppressing Range of Adaptive Stepsizes of Adam to Improve Generalisation Performance. arXiv:2302.01029 [cs.LG], 2023.
- [33] G. Zhang, K. Niwa, and W. B. Kleijn. Lookahead Diffusion Probabilistic Models for Refining Mean Estimation. In *Computer Vision and Pattern Recognition (CVPR)*, 2023.
- [34] Q. Zhang and Y. Chen. Fast Sampling of Diffusion Models with Exponential Integrator. arXiv:2204.13902 [cs.LG], 2022.

A Proof for Lemma 1

Firstly, we rewrite the update expression for \mathbf{z}_{i+1} in terms of \mathbf{z}_i , and the two estimators $\mathbf{D}_{\theta}(\mathbf{z}_i, t_i)$ and $\mathbf{D}_{\theta}(\tilde{\mathbf{z}}_{i+1}, t_{i+1})$:

$$\begin{aligned}
\mathbf{z}_{i+1} &= \mathbf{z}_i + (t_{i+1} - t_i)(0.5\mathbf{d}_i + 0.5\mathbf{d}'_i) \\
&= \mathbf{z}_i + (t_{i+1} - t_i) \left(\frac{\mathbf{z}_i - \mathbf{D}_{\theta}(\mathbf{z}_i, t_i)}{2t_i} + \frac{\tilde{\mathbf{z}}_{i+1} - \mathbf{D}_{\theta}(\tilde{\mathbf{z}}_{i+1}, t_{i+1})}{2t_{i+1}} \right) \\
&= \mathbf{z}_i + (t_{i+1} - t_i) \frac{\mathbf{z}_i - \mathbf{D}_{\theta}(\mathbf{z}_i, t_i)}{2t_i} \\
&\quad + (t_{i+1} - t_i) \frac{\mathbf{z}_i + (t_{i+1} - t_i)(\mathbf{z}_i - \mathbf{D}_{\theta}(\mathbf{z}_i, t_i))/t_i - \mathbf{D}_{\theta}(\tilde{\mathbf{z}}_{i+1}, t_{i+1})}{2t_{i+1}} \\
&\stackrel{\text{assume}}{=} \mathbf{z}_i + (t_{i+1} - t_i) \frac{\mathbf{z}_i - \bar{\mathbf{D}}_{\theta}(\mathbf{z}_i, \tilde{\mathbf{z}}_{i+1})}{t_i}.
\end{aligned} \tag{24}$$

Next, we derive the expression for $\bar{\mathbf{D}}_{\theta}(\mathbf{z}_i, \tilde{\mathbf{z}}_{i+1})$ in (24). To do so, we let

$$\begin{aligned}
\frac{\mathbf{z}_i - \bar{\mathbf{D}}_{\theta}(\mathbf{z}_i, \tilde{\mathbf{z}}_{i+1})}{t_i} &= \frac{\mathbf{z}_i - \mathbf{D}_{\theta}(\mathbf{z}_i, t_i)}{2t_i} + \frac{\mathbf{z}_i + (t_{i+1} - t_i)(\mathbf{z}_i - \mathbf{D}_{\theta}(\mathbf{z}_i, t_i))/t_i - \mathbf{D}_{\theta}(\tilde{\mathbf{z}}_{i+1}, t_{i+1})}{2t_{i+1}} \\
\Leftrightarrow \mathbf{z}_i - \bar{\mathbf{D}}_{\theta}(\mathbf{z}_i, \tilde{\mathbf{z}}_{i+1}) &= 0.5(\mathbf{z}_i - \mathbf{D}_{\theta}(\mathbf{z}_i, t_i)) + \frac{t_i \mathbf{z}_i + (t_{i+1} - t_i)(\mathbf{z}_i - \mathbf{D}_{\theta}(\mathbf{z}_i, t_i)) - t_i \mathbf{D}_{\theta}(\tilde{\mathbf{z}}_{i+1}, t_{i+1})}{2t_{i+1}} \\
\Leftrightarrow -\bar{\mathbf{D}}_{\theta}(\mathbf{z}_i, \tilde{\mathbf{z}}_{i+1}) &= -0.5\mathbf{D}_{\theta}(\mathbf{z}_i, t_i) + \frac{-(t_{i+1} - t_i)\mathbf{D}_{\theta}(\mathbf{z}_i, t_i) - t_i \mathbf{D}_{\theta}(\tilde{\mathbf{z}}_{i+1}, t_{i+1})}{2t_{i+1}} \\
\Leftrightarrow -\bar{\mathbf{D}}_{\theta}(\mathbf{z}_i, \tilde{\mathbf{z}}_{i+1}) &= -\mathbf{D}_{\theta}(\mathbf{z}_i, t_i) + \frac{t_i(\mathbf{D}_{\theta}(\mathbf{z}_i, t_i) - \mathbf{D}_{\theta}(\tilde{\mathbf{z}}_{i+1}, t_{i+1}))}{2t_{i+1}} \\
\Leftrightarrow \bar{\mathbf{D}}_{\theta}(\mathbf{z}_i, \tilde{\mathbf{z}}_{i+1}) &= \mathbf{D}_{\theta}(\mathbf{z}_i, t_i) + \frac{t_i(\mathbf{D}_{\theta}(\tilde{\mathbf{z}}_{i+1}, t_{i+1}) - \mathbf{D}_{\theta}(\mathbf{z}_i, t_i))}{2t_{i+1}}
\end{aligned}$$

The proof is complete.

B Hyper-parameters of IIA when minimizing MSEs

Table 1: Parameter-setups of IIA in MMSE in BIIA-EDM and IIA-EDM. The four pre-trained models below are downloaded from the official open source repository of the work [12].

pre-trained models	BIIA-EDM	IIA-EDM
edm-cifar10-32x32-cond-vp.pkl	$(M, r) = (3, 1)$	$(M, r) = (3, 1)$
edm-ffhq-64x64-uncond-vp.pkl	$(M, r) = (3, 0)$	$(M, r) = (3, 1)$
edm-afhqvc2-64x64-uncond-vp.pkl	$(M, r) = (3, 1)$	$(M, r) = (3, 1)$
edm-imagenet-64x64-cond-adm.pkl	$(M, r) = (3, 1)$	$(M, r) = (3, 1)$

For the experiment of IIA-DDIM, IIA-SPNDM, and IIA-IPNDM, the hyper-parameters were set $(M, r) = (3, 1)$.

C Performance of IIA-SPNDM and IIA-IPNDM

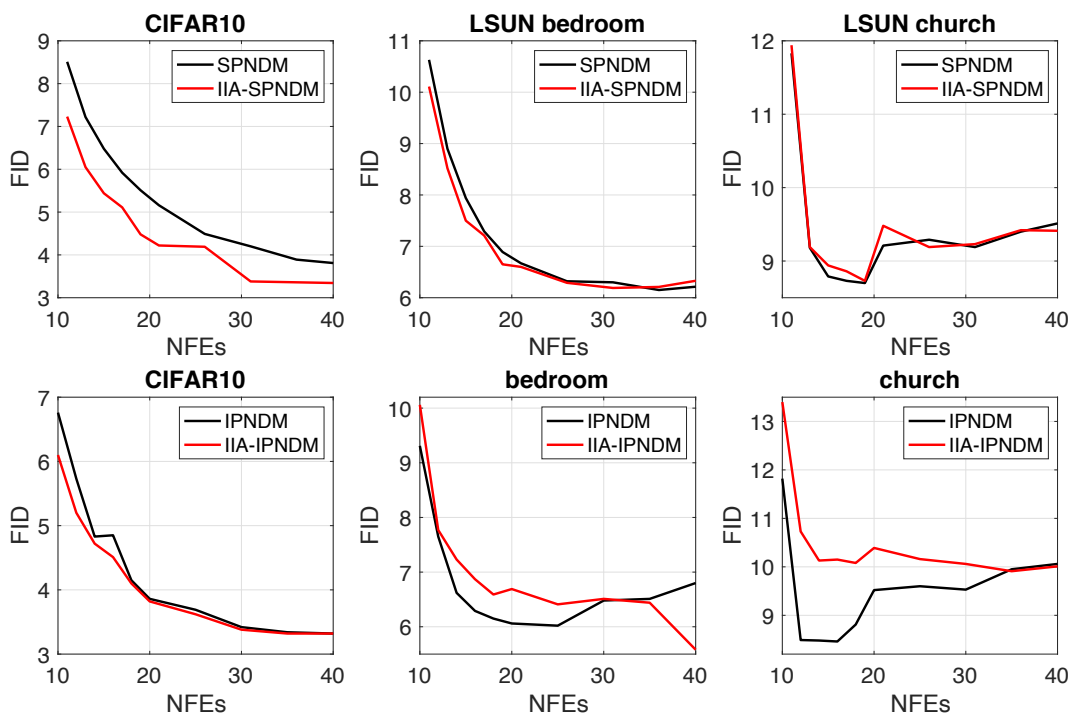


Figure 4: Performance of four sampling methods.